Available online at www.sciencedirect.com
ScienceDirect
Journal of Membrane Science 285 (2006) 272–281
journal of MEMBRANE SCIENCE
www.elsevier.com/locate/memsci

Effect of membrane structure on mass-transfer in the membrane gas–liquid contacting process using microporous PVDF hollow fibers

Supakorn Atchariyawut [a], Chunsheng Feng [b], Rong Wang [c,*], Ratana Jiraratananon [a], D.T. Liang [c]

[a] *Department of Chemical Engineering, King Mongkut's University of Technology Thonburi, Bangkok 10140, Thailand*
[b] *School of Civil and Environmental Engineering, Nanyang Technological University, Singapore 639798, Singapore*
[c] *Institute of Environmental Science & Engineering, Nanyang Technological University, Innovation Center (NTU), Block 2, Unit 237, 18 Nanyang Drive, Singapore 637723, Singapore*

Received 8 June 2006; received in revised form 8 August 2006; accepted 26 August 2006
Available online 1 September 2006

Abstract

In order to gain a better understanding of the membrane's role in the whole process of mass-transfer in membrane gas–liquid contacting systems, PVDF microporous hollow fiber membranes have been fabricated using three different dope solutions containing *N*-methyl-2-pyrrolidone (NMP) and different additives. The resultant hollow fibers with different structures were used to make membrane modules, which were then applied as gas–liquid membrane contactors for CO_2 absorption in water. The membranes were characterized and the effect of membrane structure on the mass-transfer was analysed accordingly.

It was found that the additives used imposed a significant effect on the final membrane structure under the same spinning conditions. Compared with distilled water, phosphorous acid and glycerol showed a stronger pore-inducing ability. As a result, the membrane #1 or #2 made by the dope with phosphorous acid or glycerol as an additive had a larger pore size and a higher value of MWCO. The finger-like pores also occupied a larger portion on the membranes #1 and #2 than on the membrane #3, which used distilled water as an additive. Moreover, the membranes #1 and #2 presented a much wider pore size distribution than the membrane #3.

The different membrane structures turned out to affect CO_2 absorption performance when used as contactors. Since the ratio of the membrane resistance over the overall mass-transfer resistance was increased in the order of #1 < #2 < #3, with respect to the reductions of MWCO and the finger-like pore portion of these three membranes in the same sequence, the CO_2 absorption performance was in the sequence of #1 > #2 > #3. In addition, it was noticed that all the membranes exhibited considerable membrane resistances from 22% to 36% though the model system used was pure CO_2 absorption in distilled water. The partial wetting was probably caused by the capillary condensation of water vapour in the membrane pores instead of water penetration, as the experiment shows that the CO_2 flux of three PVDF membranes was kept almost unchanged over 15 days of operation. In comparison with a commercial double skin layer PVDF membrane, it was found that the membrane with an inner skin-free structure plus a porous substrate is favourable to be used in the membrane gas–liquid contacting process.

Keywords: PVDF hollow fibers; Membrane structure; Mass-transfer resistance; Membrane contactors; Carbon dioxide capture

1. Introduction

Hydrophobic microporous membranes have attracted increasing attention in recent years for use as contactors in chemical absorption to remove CO_2, H_2S, SO_2 from flue and natural gases [1,2], and in membrane distillation processes for desalination [3,4]. Despite certain downside such as the addition of an extra mass-transfer resistance caused by the membrane, the microporous hollow fiber membrane contactors offer a lot of advantages including individual gas and liquid flow channels, a compact modular structure to provide huge gas–liquid interfaces and operational flexibility to scale up or down [1].

For a gas–liquid absorption process, an aqueous absorbent flows on one side of the membrane while the feed gas flows on the other side of the membrane. The microporous membrane pores can be filled either by the liquid or by the gas or by both of them.

* Corresponding author. Tel.: +65 6794 3764; fax: +65 6792 1291.
E-mail address: rwang@ntu.edu.sg (R. Wang).

0376-7388/$ – see front matter © 2006 Elsevier B.V. All rights reserved.
doi:10.1016/j.memsci.2006.08.029

It is well recognized that if the membrane pores are gas-filled, i.e. the operation is at the non-wetted mode, the system can achieve higher performance by taking the advantage of the higher gas diffusivity [2,5]. Therefore, hydrophobic materials are preferred to be used to make membranes so that the aqueous absorbent solution tends to be repelled at the hollow fiber membrane pore mouths.

Among various hydrophobic polymers, polypropylene (PP) and polytetrafluoroethylene (PTFE) are the most popular membrane materials. However, since PTFE and PP membranes are usually produced by stretching or thermal methods, the relatively low porosity of PP and PTFE membranes restricts a significant increase on absorption flux. Consequently, the main advantage of the microporous hollow fiber membrane, i.e. a high area-to-volume ratio, cannot be fully exerted. In fact, hydrophobic microporous hollow fiber membranes with high porosity can be formed by a simple and convenient method of non-solvent induced phase inversion separation (NIPS) process, and membrane structure and morphology can also be optimized by adjusting various preparation conditions if a suitable solvent can be found for the selected polymer. Although PTFE and PP are excluded on account of their insolubility in common solvents, polyvinylidene fluoride (PVDF), another strong hydrophobic polymer with excellent chemical and thermal resistances, has been successfully employed for making membranes by this approach [6–8].

Unlike symmetric PTFE and PP membranes, the PVDF hollow fiber membrane prepared by the NIPS process can exhibit an asymmetric structure with a dense selective layer plus a porous substrate. The membrane pore size and pore size distribution in the dense layer, which is normally in direct contact with the liquid, are important factors associated with membrane wetting problem except for the membrane surface property (hydrophobicity), the nature of the liquid-phase and operating conditions [9]. In addition, the most of mass-transfer resistance in the membrane is attributed to the dense layer, while the porous substrate only provides mechanic support and fractional resistance.

To determine the membrane mass-transfer resistance, Wilson plot is one of the methods which are widely applied in membrane contactor systems. Rangwala [10] determined PP membrane mass-transfer coefficient for CO_2 capture with water and other absorbents by using Wilson plot method. Prasad and Sirkar [11] also used the same approach to determine the membrane resistance in liquid extraction process for both hydrophobic and hydrophilic hollow fiber membranes. The recent report from Mavroudi et al. [12] examined the change of mass-transfer resistance with time for CO_2 absorption in water in PP hollow fiber membrane module. It was found that the experimental absorption flux declined significantly with time, which was attributed to gradual partial pore filling by liquid. The partially wetted membrane led to an increase of membrane resistance being 21–53% of total resistances.

In the present work, PVDF material was selected to prepare three different dope solutions containing *N*-methyl-2-pyrrolidone (NMP) and different additives for hollow fiber fabrication. The resultant hollow fibers were used to make membrane modules, which were then applied as gas–liquid membrane contactors for a model system of CO_2 absorption in water. The different membrane structures resulted from the addition of different additives in the polymer dopes were characterized and discussed. The analysis of membrane mass-transfer resistance of in-house made PVDF membranes was also carried out in order to gain a better understanding of the membrane's role in the whole process of mass-transfer in the membrane contactors and guide further improvement on PVDF membrane fabrication.

2. Theory

2.1. Resistance-in-series model

Fig. 1 depicts the mass-transfer mechanism of a non-wetted (gas-filled pores) gas–liquid membrane contactor. It can be seen that the feed gas has to encounter with three resistances in series, i.e. gas phase boundary layer, membrane and liquid-phase boundary layer. Thus, the resistance-in-series equation is employed to describe the mass-transfer in the system, which can be written as follows [13]:

$$\frac{1}{K_{ol}} = \frac{1}{k_l} + \frac{Hd_o}{k_m d_{ln}} + \frac{Hd_o}{k_g d_i} \tag{1}$$

where K_{ol} is the overall mass-transfer coefficient based liquid-phase ($m\,s^{-1}$), k_l, k_m, k_g are the individual mass-transfer coefficient of liquid-phase, membrane and gas phase, respectively. H represents Henry's constant and is 0.831 for water [14]. d_i, d_o, d_{ln} are the inner, outer and logarithmic mean diameters of membrane, respectively.

The overall mass-transfer coefficient, K_{ol}, can be calculated based on experiments by the following equation [15]:

$$K_{ol} = \frac{Q_l(C_{l,out} - C_{l,in})}{A_T \Delta C_{l,av}} \tag{2}$$

The logarithmic mean concentration, $\Delta C_{l,av}$, is expressed as

$$\Delta C_{l,av} = \frac{(HC_{g,in} - C_{l,out}) - (HC_{g,out} - C_{l,in})}{\ln(HC_{g,in} - C_{l,out})/(HC_{g,out} - C_{l,in})} \tag{3}$$

where A_T is the gas–liquid contact area; $C_{l,in}$, $C_{l,out}$ liquid-phase inlet and outlet concentrations; $C_{g,in}$, $C_{g,out}$ gas phase inlet and outlet concentrations, Q_l is the liquid volumetric flow rate.

2.2. Individual mass-transfer coefficients

The Lévêque's correlation is widely used to predict accurately the tube side mass-transfer coefficient [1,16]:

$$Sh = 1.62\left(\frac{d_i^2 V}{LD}\right)^{1/3} \tag{4}$$

where Sh is Sherwood number, D the diffusion coefficient of the fluid in the tube, L the tube length and V is the fluid velocity.

There are many correlations proposed to determine the shell side mass-transfer coefficient [11,16,17]. However, each of them

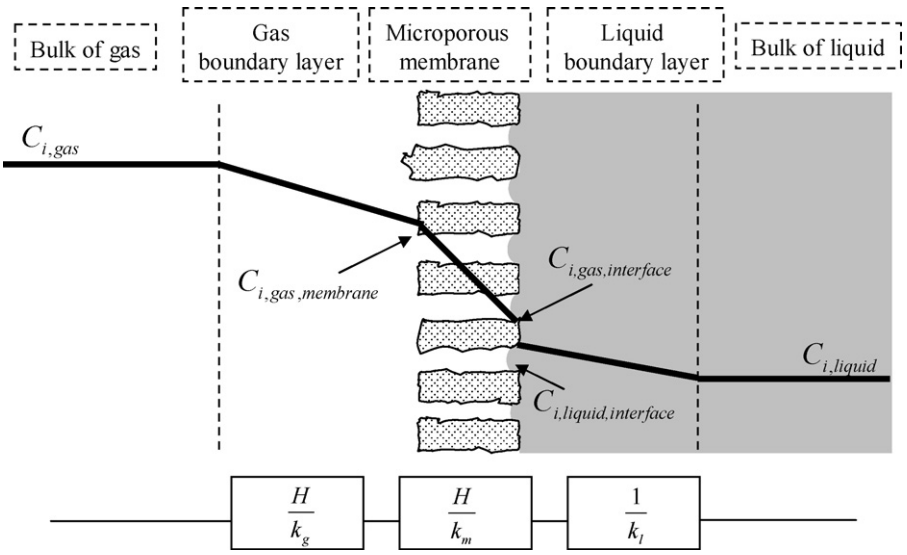

Fig. 1. Mass-transfer regions and resistance-in-series in non-wetted membrane contactors.

is applicable to a certain limited range of operation. In general, it can be expressed in the following form:

$$Sh = aRe^{\alpha} Sc^{\beta} \tag{5}$$

where *Re* and *Sc* are Reynolds and Schmidt numbers, respectively. For the liquid flow in the shell side of membrane, Eq. (5) can be simplified to

$$k_l = C_1 V^{\alpha} \tag{6}$$

As for the membrane mass-transfer coefficient in a completely non-wetted case, it can be calculated using the following equation [12]:

$$k_m = \frac{D_{g,eff}\varepsilon_m}{\tau_m l_m} \tag{7}$$

where $D_{g,eff}$ is the effective diffusion coefficient of pure gas filled into the pores. It is calculated from the summation between the molecular self-diffusion coefficient and the diffusion coefficient which is the interaction of gas molecules and membrane wall. ε_m, τ_m, and l_m are the porosity, tortuosity, and thickness of the membrane, respectively.

2.3. Wilson plot

The Wilson plot is drawn by $1/K_{ol}$ versus $1/V^{\alpha}$ based on Eqs. (1) and (6). The value of α is chosen for achieving the best straight line. In the gas–liquid membrane contacting process, if the resistance in the gas phase is much smaller than the total resistance, the H/k_g in Eq. (1) becomes negligible. Thus, the interception of the Wilson plot represents the value of membrane mass-transfer resistance.

2.4. Pore size and pore flux distributions of hollow fiber membranes

The most common form of the two-parameter log-normal distribution function, $f(d)$, is taken to describe the pore size distribution of the membrane:

$$f(d) = \frac{1}{\ln(\sigma)d\sqrt{2\pi}} \exp\left[-\frac{1}{2}\left(\frac{\ln(d/D^*)}{\ln(\sigma)}\right)^2\right] \tag{8}$$

The pore flux distribution function $f_f(d)$ can be given accordingly

$$f_f(d) = \left(\frac{d}{D^*}\right)^4 \frac{1}{\ln(\sigma)d\sqrt{2\pi}} \times \exp\left[-\frac{1}{2}\left(\frac{\ln(d/D^*)}{\ln(\sigma)}\right)^2 - 8(\ln\sigma)^2\right] \tag{9}$$

where D^*, σ are the geometric mean diameter and the geometric standard deviation, respectively.

Since the retention coefficient of a solute $R(a)$ can be derived theoretically based on the pore size distribution parameters, or gained from the measurement of the rejection characteristics of dextran through the membrane, D^* and σ can be obtained by solving the minimization problem (Eq. (10)) using the Levenberg–Marquardt algorithm [18]:

$$\left(\sum_{i=1}^{N}\{R(a_i)|_{Exp.} - R(a_i)|_{Cal.}\}^2\right)\Bigg|_{MIN} \rightarrow (D^*, \sigma) \tag{10}$$

3. Experimental

3.1. Membrane material and chemicals

The membrane material, PVDF (Kynar grade 740, molecular weight: 156,000, pellet form), is a commercial polymer and was purchased from Elf Autochem (USA). *N*-Methyl-2-pyrrolidone (NMP, >99.5%, CAS#: 872-50-4) supplied by Merck was used as a solvent. Phosphorous acid (98+%, A Johnson Matthey Company, Alfa Aesar, Lancaster) and glycerol (99.0%, Cica-Reagent, Kanto Chemical Co. Inc., Japan) were the non-solvent additives. Some dextran $(C_6H_{10}O_5)_n$ samples

with different molecular weights (1500–400,000; CAS# 9004-54-0; from Fluka and Sigma) were used to characterize the molecular weight cut-off (MWCO) of hollow fiber membranes. All the reagents were used as received.

3.2. Fabrication of asymmetric PVDF hollow fiber membranes

Hollow fiber membranes were formed by NIPS process. Three batches of polymer dope solutions were prepared. The difference of the three dope solutions lies in the addition of different additives: one consists of 17 wt.% PVDF, 3 wt.% phosphorous acid and 80 wt.% NMP; another consists of 17 wt.% PVDF, 3 wt.% glycerol and 80 wt.% NMP; the third is 17 wt.% PVDF, 3 wt.% distilled water and 80 wt.% NMP. The polymer dopes were dissolved at 90 °C by stirring for several days until homogenous and stable solutions were formed. The resulting solution was filtered to remove remnant contaminants, then, degassed about 24 h at room temperature. The dope after treatment was connected with N_2 gas cylinder that offered certain pressure to extrude the dope out the spinneret, and then to be immersed into tap water. A mixture of distilled water (20 wt.%) and NMP (80 wt.%) was used as the bore fluid, or else reported. The selection of such a solvent content in the bore fluid is aimed to yield hollow fiber membranes with an open and porous inner skin layer. It is possible to produce microporous membranes by adding solvent to the coagulation bath [19] and the phase inversion was initiated when the water weight fraction ($W_{H_2O}/(W_{H_2O} + W_{NMP})$) is about 9.0–9.5 wt.% for the PVDF/NMP/H_2O system [18]. In order to prevent shrinkage of the nascent membrane during drying process, the hollow fiber membranes were subjected to solvent exchange, this was, the membrane was immersed in turn into water/ethanol (1:1), pure ethanol, ethanol/*n*-hexane (1:1) over 24 h. In the process, water in the membrane pores was gradually replaced with ethanol or other mixtures possessing lower surface tension. The membranes were subsequently dried at room temperature before characterization tests.

3.3. Measurement of hollow fibers' pure water flux and MWCO

The wet hollow fibers were cut into a length of 30 cm, and small test modules were made with 8–10 pieces of fibers in a glass tube with an effective length of 25 cm. The Milli-Q ultrapure water was circulated through the shell side of the membrane modules to test the pure water flux. The details of test procedure were described in Ref. [18].

The membrane pore size was characterized based on the filtration of a dextran solution containing approximately 1500 ppm of mixed dextran in salt-free Milli-Q water. The molecular weight distribution of the mixed dextran varies from 1000 to 400,000 Da. In this experiment, the feed flux was controlled at around 1.1 L/min and the operation pressure was controlled at 0.5 bar to eliminate concentration polarization. The dextran molecular weight distribution in the feed and permeate solutions were measured by gel permeation chromatography (GPC) on a Waters chromatography system (the ultrahydrogel columns 120, 250, 500). The details of the experiments can be found elsewhere [18].

3.4. Measurement of CO_2 absorption in the membrane contactor

The glass modules containing 15 pieces of PVDF fibers with an effective length of 25 cm were also prepared as membrane contactors for CO_2 absorption experiments. Prior to the test, the modules were heated around 110 °C for overnight to remove moisture. Pure CO_2 was used as the feed gas while the N_2 saturated distilled water was employed as the absorbent. The liquid passed through the shell side and the gas flowed countercurrently through the lumen side of the hollow fibers, as the selective layers of PVDF hollow fibers were in the outer surfaces. Experimental data were recorded after the contactor system was stabilized. The detailed experimental setup and test procedures could be found elsewhere [20].

3.5. Scanning electron microscopy (SEM) and membrane porosity measurements

The morphologies of the hollow fiber membranes were captured using SEM. The dried membrane samples were broken in liquid nitrogen and then dried again at 80 °C in a vacuum oven for 1 day. The membrane samples were sputtered with a thin layer of gold using a SPI-Module sputter coater. The cross-section and inner surface of hollow fiber membranes were examined using a JEOL JSM-5310LV scanning electron microscope (SEM).

The membrane porosity, ε_m, was defined as the volume of the pores divided by the total volume of the membrane. It can usually be determined by gravimetric method, measuring the weight of liquid (here isopropyl alcohol from VWR company, analytical reagent) contained in the membrane pores:

$$\varepsilon_m = \frac{(w_1 - w_2)/D_i}{(w_1 - w_2)/D_i + w_2/D_p} \quad (11)$$

where w_1 is the weight of the wet membrane; w_2 the weight of the dry membrane; D_i the isopropyl alcohol density; D_p is the polymer density.

4. Results and discussion

4.1. Effect of polymer dope component on the hollow fiber membrane structure

The morphology of hollow fiber membranes formed by NIPS method strongly depends upon polymer dope components and preparation conditions. Fig. 2 shows cross-section structures of three in-house made PVDF hollow fibers from different preparation systems and one commercial PVDF sample as a reference, while Table 1 lists corresponding dope information and spinning conditions. The commercial sample denoted as membrane #T, which had double dense skin layers because of water being the coagulant and the bore fluid, was kindly provided by Tianjin

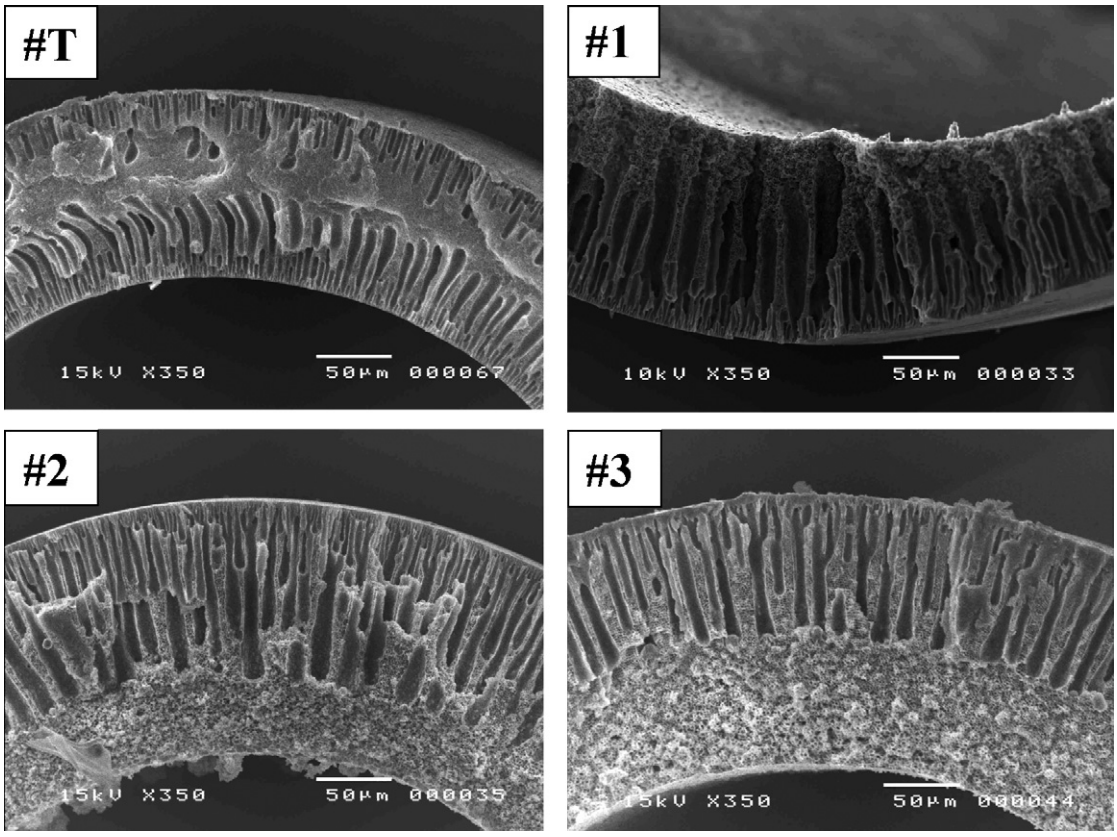

Fig. 2. Cross-section images of four PVDF hollow fiber membranes (membrane #T: a commercial sample and membranes #1 to #3: in-house made hollow fibers).

Motian Membrane Eng. & Tech. Co. Ltd., China. It can be seen that when a mixture containing 20 wt.% of distilled water and 80 wt.% of NMP was used as the bore fluid, the membranes did not exhibit inner dense skin layers, as shown in the pictures of the membranes #1 to #3. The internal skin removal was ascribed to the slower phase inversion in the fiber inner side caused by the weak internal coagulant. Meanwhile, the existence of outer dense skin layer was still captured for water was used as an external precipitant. Moreover, a close look revealed that the finger-like pores on the membrane #1 are much longer than that on sample #3. Since all the fabrication conditions were kept the same except for the type of additive used, the difference in the membrane structure should be attributed to the additive.

It is well known that the formation of asymmetric membranes depends on both thermodynamic and kinetic parameters. The three additives, phosphorous acid, glycerol and water, are non-solvents to the PVDF. Their additions into the polymer dope will reduce the thermodynamic miscibility of the dope solution and thus enhance the liquid–liquid-phase separation (thermodynamic effect). On the other hand, the additives also increase the dope viscosity, which affects the mutual diffusion between the solvent and non-solvent (kinetic effect). In addition, the increase in dope viscosity also indicates the existence of stronger interactions among the components of the polymer dope (thermodynamic effect). Therefore, the impact of the additive on the membrane structure is due to the combined factors [21].

Table 1
Spinning conditions of batches #1 to #3

	Batch #1	Batch #2	Batch #3
Spinning dope composition	17% PVDF; 3% phosphorous acid; 80% NMP	17% PVDF; 3% glycerol; 80% NMP	17% PVDF; 3% distilled water; 80% NMP
Bore fluid (w/w)	NMP/H_2O: 80/20	NMP/H_2O: 80/20	NMP/H_2O: 80/20
External coagulation bath	Tap water	Tap water	Tap water
Dope flow rate (g/min)	14	14	14
Bore fluid rate (mL/min)	4	4	4
Air gap (mm)	5	5	5
Spinning dope temperature (°C)	25	25	25
Bore temperature (°C)	25	25	25
External coagulation temperature (°C)	Room temperature	Room temperature	Room temperature

Table 2
Characters of in-house made PVDF membranes

Membrane	Outer radius (μm)	Inner radius (μm)	Pure water flux ($L\,m^{-2}\,h^{-1}\,atm^{-1}$)	MWCO (Da)	Pore size distribution (calculated)		Porosity ε_m (%)
					D^* (nm)	σ	
#1	414	257	90	290,000	20.0	1.216	76.02
#2	485	286	52	110,000	9.25	1.385	74.02
#3	514	300	28	45,000	11.1	1.088	69.88

Our experiments show that when a 3.0 wt.% additive was added into the dope, the dope viscosity was increased in the sequence of dope #1 (phosphorous acid) > dope #2 (glycerol) > dope #3 (water), which reveals that there was a strongest interaction among phosphorous acid, NMP and/or PVDF. In fact, phosphorous acid and NMP formed a stronger acid–base complex than water and NMP. The MWCO data in Table 2 suggest that the membrane #1 possessed the largest pore size on the outer surface, which promoted more intensive influx of external coagulant (water) into the dope. With a more rapid phase inversion rate, the finger-like pores tended to grow into a deeper sublayer.

Fig. 3 shows the inner surfaces of the membranes #1 to #3 in comparison with that of the membrane #T. The in-house made membranes presented bigger pore conformation than the membrane #T which used water as the bore fluid. The inner surfaces of the membranes #1 to #2 presented more porous structures than the membrane #3, which implies that phosphorous acid and glycerol possessed a stronger pore-inducing ability than water at current experiment conditions.

4.2. Pore size and flux distributions of PVDF hollow fiber membranes

Fig. 4 depicts the rejection characteristic of in-house made PVDF hollow fiber membranes. The MWCO was around 290, 110 and 45 kDa for the membranes #1, #2 and #3, respectively, which are tabulated in Table 2 along with the pore size distribution parameters (D^*, σ) and porosity of the three membranes. It can be seen that the geometric standard deviation (σ) of the membrane #3 using 3 wt.% distilled water as the pore former was smaller than that using phosphorous acid or glycerol at the same concentration as the pore former, which suggests a much narrower pore size distribution of membranes obtained from batch #3 dope. This result can be observed more directly from Fig. 5.

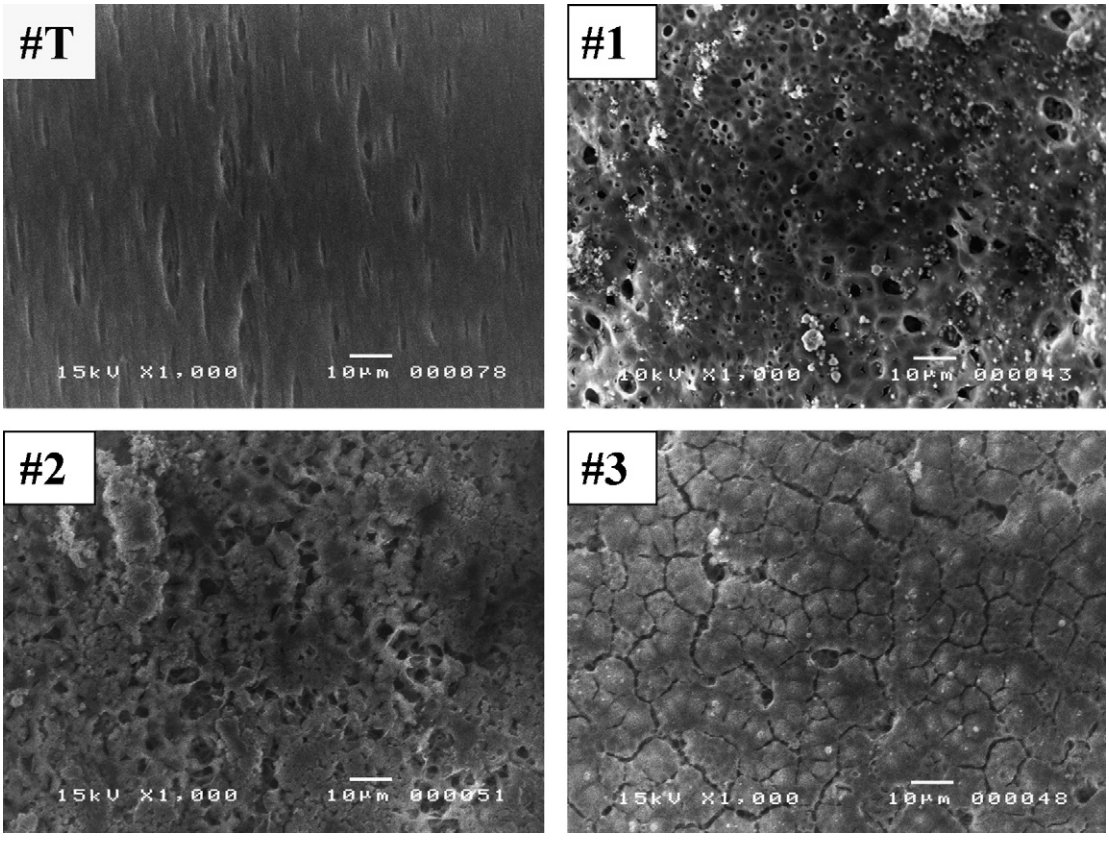

Fig. 3. Inner surfaces of four PVDF hollow fiber membranes (membrane #T: a commercial sample and membranes #1 to #3: in-house made hollow fibers).

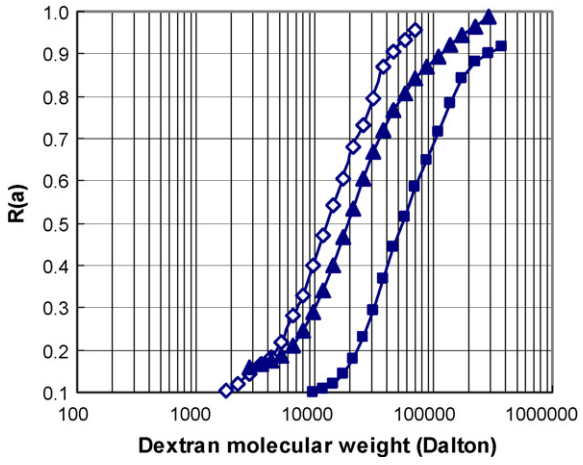

Fig. 4. Rejection characterization of in-house made hollow fiber membranes (■: membrane #1, ▲: membrane #2, and ◊: membrane #3).

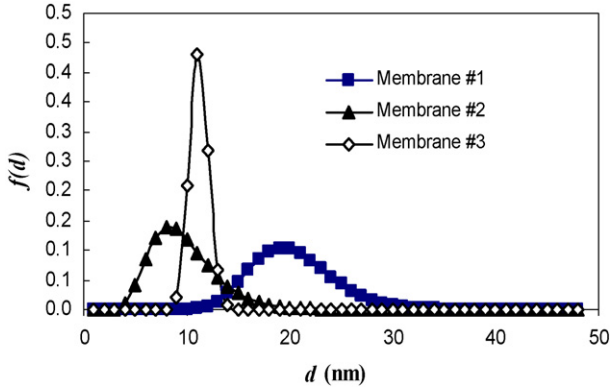

Fig. 5. The pore size distribution $f(d)$ of in-house made hollow fiber membranes.

Fig. 6 illustrates the pore flux distributions of the three membranes. The peaks of the flux distribution curve $f_f(d)$ shifted towards right side of x-axis compared with the pore size distribution curve $f(d)$, suggesting that the small portion of big pores made a considerable contribution to the flux. Besides, the pore flux was spread apart much wider if the pore size distribution was wide. That was why the pure water flux of the membrane #2 was larger than that of the membrane #3, though the mean pore size of the membrane #2 was a bit smaller that that of the membrane #3.

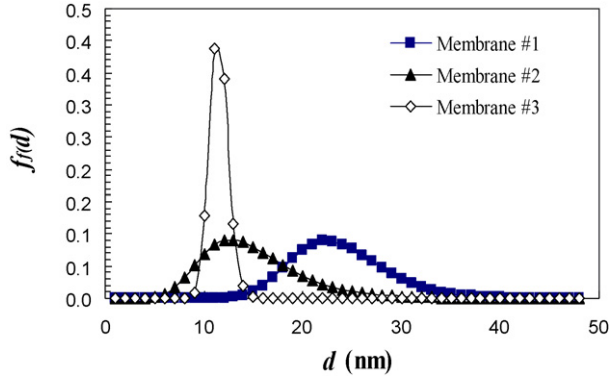

Fig. 6. The pore flux distribution function $f_f(d)$ of in-house made hollow fiber membranes.

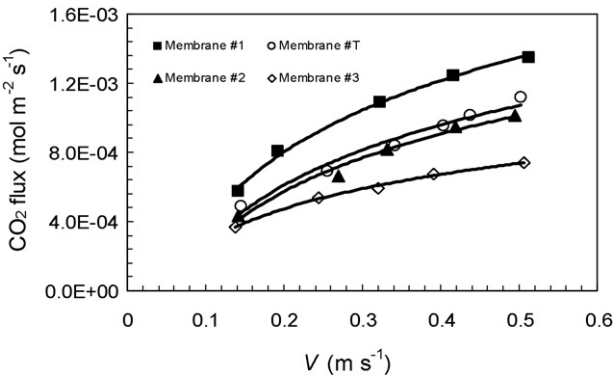

Fig. 7. Effect of liquid velocity on the CO_2 flux of four different PVDF membranes (pure CO_2–pure water system).

4.3. Effect of the hollow fiber membrane structure on mass-transfer resistance

Membranes prepared with different dope solutions showed different structures, which turned out to affect CO_2 absorption performance when used as contactors. Fig. 7 shows CO_2 flux versus liquid velocity for four different types of PVDF membranes. The CO_2 flux increased with an increase in liquid velocity for either membrane, as the consumed distilled water by CO_2 was replaced by more fresh water when the absorbent was supplied at a higher speed. In addition, it was observed that for in-house made PVDF hollow fiber membranes, the CO_2 absorption performance was in the sequence of #1 > #2 > #3 with respect to the same order of MWCO of these three membranes. Moreover, the membrane #1 presented even better performance than the membrane #T though the membrane #T has the largest mean pore size, as given in Table 3. Obviously, an inner skin-free structure with a sufficient fraction of pores in the substrate is favourable to the gas transport.

The effect of membrane structure on the system performance can be indicated quantitatively by the membrane resistance. Fig. 8 shows the Wilson plot of $1/K_{ol}$ versus $V^{-0.93}$ for the four types of PVDF membranes. The α value of 0.93 was found to

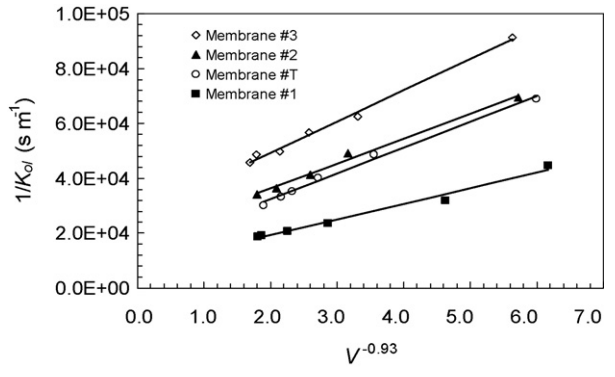

Fig. 8. Wilson plot of four different PVDF membranes (pure CO_2–pure water system).

Table 3
Analysed membrane resistances from Wilson plot method (pure CO_2–pure water system)

Type of membranes	Characteristics of membranes	Overall mass-transfer resistance[a] $R_{total} = 1/K_{ol}$ (s/m)	Analysed membrane resistance $R_m = Hd_o/k_m d_{ln}$ (s/m)	R_m/R_{total} (%)	Mean pore size (μm)
#T	PVDF asymmetric double skin layers	47,653	13,565	28.5	0.20[b]
#1	PVDF asymmetric single skin layer	28,589	7,930	27.7	0.020
#2	PVDF asymmetric single skin layer	51,101	18,295	35.8	0.009
#3	PVDF asymmetric single skin layer	67,879	26,558	39.1	0.011
#4 [15]	PP symmetric structure	21,669	4,733	21.8	0.04[b]
#5 [12]	PP symmetric structure	25,500[c]	5,500	21.6	0.05[b]

[a] R_{total} was achieved at $V = 0.25\ m\ s^{-1}$.
[b] Provided by manufacturers.
[c] Achieved at $Q_l = 5.67 \times 10^5\ m^3/s$.

present the best straight line of Wilson plot:

$$\text{membrane \#1}: \quad \frac{1}{K_{ol}} = 5691.0V^{-0.93} + 7930.9, \quad R^2 = 0.981 \tag{12}$$

$$\text{membrane \#2}: \quad \frac{1}{K_{ol}} = 9037.5V^{-0.93} + 18295, \quad R^2 = 0.991 \tag{13}$$

$$\text{membrane \#3}: \quad \frac{1}{K_{ol}} = 11383V^{-0.93} + 26558, \quad R^2 = 0.994 \tag{14}$$

$$\text{membrane \#T}: \quad \frac{1}{K_{ol}} = 9390.7V^{-0.93} + 13565, \quad R^2 = 0.993 \tag{15}$$

Yang and Cussler also correlated $1/K_{ol}$ with $V^{-0.93}$ to describe the gas absorption in the membrane module where the liquid was in shell side flow parallel to the fibers [16]. Based on Eqs. (11)–(15), the membrane mass-transfer coefficients can be obtained via the interceptions of these equations.

The membrane resistances of the membranes #1 to #3 and #T are summarized in Table 3. For comparison, the membrane mass-transfer resistances of two PP membranes were also listed in the table. For PP membrane #4 [15], the membrane mass-transfer resistance was calculated using their experimental data, but $\alpha = 0.33$ based on Lévêque's correlation was selected to be the power of liquid velocity to provide a best straight line with $R^2 = 0.99$, as distilled water was fed through the lumen side of the fibers. As for PP membrane #5 [12], the membrane mass-transfer resistance was cited directly, which was obtained at the lowest liquid flow rate of their experiments.

Surprisingly, from Table 3 it was noticed that all the membranes exhibited considerable membrane resistances though the model system used was pure CO_2 absorption in distilled water. The membrane resistances of the PVDF membranes #T and #1 to #3 occupied around 28–36% of the total resistances. Even for the commercial Celgard PP membranes, around 22% of the total resistances were attributed to the membrane. In fact, according to Eq. (7), if the membrane is completely gas-filled, the membrane resistance should be less than 0.5%. Clearly, all the membranes were partially wetted by water. However, our experiment (Fig. 9) shows that the CO_2 flux of three PVDF membranes was kept almost unchanged over 15 days of operation.

Basically, water can enter a porous material either as liquid or vapour. While the first case is a result of capillarity and/or infiltration, the latter can be achieved by capillary condensation in pores [22]. PVDF and PP materials are hydrophobic in nature and the pores sizes of these membranes are also quite small except for the membrane #T. Based on the result shown in Fig. 9, it is unlikely that distilled water have penetrated into the membrane pores through the surface. The partial wetting was probably caused by the capillary condensation of water vapour in the membrane pores [9] and an equilibrium was then achieved within the initial short period of operation. As such, these PVDF membranes could maintain constant long-term performances after an initial flux drop. Mavroudi et al. reported that the initial wetting of the PP membrane might happen within 2–3 h when contacting with water [12].

Referring to Table 3 again, the ratio of the membrane resistance over the overall mass-transfer resistance was increased in the order of #1 < #2 < #3, corresponding to the decreases of the MWCO (Table 2) and the finger-like pore portion (Fig. 2) of these three membranes in the same sequence. With the reduction of the membrane pore size, the membrane porosity tended to decrease as shown in Table 2. A similar observation was reported

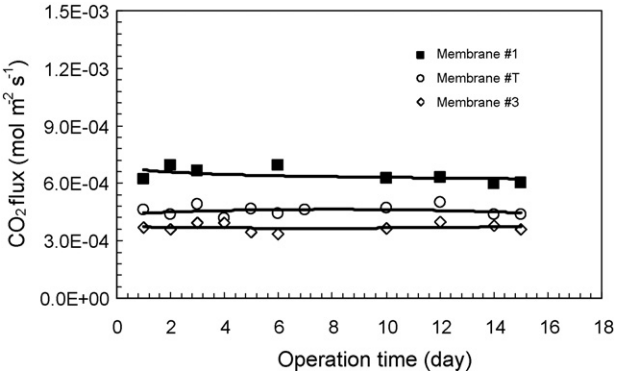

Fig. 9. Performance of three PVDF membrane modules over 15 days (pure CO_2–pure water system and $V = 0.15\ m\ s^{-1}$).

in a literature [23]. This factor promoted an increase on the membrane resistance. In addition, the smaller pore size is favourable to the capillary condensation of water vapour based on Kelvin equation, which predicts that undersaturated vapours will condense in channels of sufficiently small dimensions [22].

It was also observed that the membrane #T possessed a similar portion of membrane resistance as the membrane #1 though it had the largest mean pore size. The double skin layers on the membrane #T are believed to exert a significant resistance to the mass-transfer, in contrast to the least membrane resistance of around 22% presented by symmetric PP membranes without any dense skin layer. Nevertheless, the critical entry pressure of the absorbent solution into the membrane pores will sharply decrease with an increase on the membrane pore size, resulting in the deterioration of the long-term performance of the membrane module. Given attention to the membrane resistance and the membrane wetting by penetration, it seems that the membrane with a dense skin layer plus a porous substrate has the potential to keep an ideal long-term performance under a high absorption flux.

5. Conclusions

PVDF microporous hollow fiber membranes have been fabricated using three different dope solutions containing *N*-methyl-2-pyrrolidone (NMP) and different additives. The resultant hollow fibers with different structures were used to make membrane modules, which were then applied as gas–liquid membrane contactors for CO_2 absorption in water. The membranes were characterized and the effect of membrane structure on the mass-transfer was analysed accordingly.

It was found that the additives used imposed a significant effect on the final structure of the hollow fiber membrane under the same spinning conditions. Compared with distilled water, phosphorous acid and glycerol showed a stronger pore-inducing ability. As a result, the membrane #1 or #2 made by the dope with phosphorous acid or glycerol as an additive had a larger pore size and a higher value of MWCO. The finger-like pores also occupied a larger portion than on the membrane #3, which used distilled water as an additive. Moreover, the membranes #1 and #2 presented a much wider pore size distribution than the membrane #3.

The different membrane structures turned out to affect CO_2 absorption performance when used as contactors. The CO_2 absorption performance was in the sequence of #1 > #2 > #3, as the ratio of the membrane resistance over the overall mass-transfer resistance was increased in the order of #1 < #2 < #3, with respect to the reductions of MWCO and the finger-like pore portion of these three membranes in the same sequence. In comparison with a commercial double skin layer PVDF membrane, it was found that an inner skin-free structure with a porous substrate is favourable to the gas transfer.

In addition, it was noticed that all the membranes exhibited considerable membrane resistances from 22% to 36% though the model system used was pure CO_2 absorption in distilled water. The partial wetting was probably caused by the capillary condensation of water vapour in the membrane pores instead of water penetration, as our experiment shows that the CO_2 flux of three PVDF membranes was kept almost unchanged over 15 days of operation.

Acknowledgements

The authors from Thailand wish to thank the Thailand Research Fund and the Royal Golden Jubilee Ph.D. Program for financial support, the Institute of Environmental Science and Engineering (IESE) of Singapore for hospitality and guidance, and Prof. Neal T.S. Chung of National University of Singapore for his kind help. The authors from Singapore gratefully acknowledge the support of Agency of Science, Technology and Research of Singapore (A*STAR) for funding this research with the grant number of 032 101 0024. The authors also thank Dr. Zhang Hongyan for useful discussion and help.

Nomenclature

A_T	mass-transfer area based on outside surface area of gas–liquid contact (m^2)
C_l	concentration of carbon dioxide in the liquid-phase ($mol\,m^{-3}$)
$\Delta C_{l,av}$	logarithmic mean concentration difference of carbon dioxide in the liquid-phase ($mol\,m^{-3}$)
C_g	concentration of carbon dioxide in the gas phase ($mol\,m^{-3}$)
d_i	inside diameter of membrane (m)
d_{ln}	logarithmic mean diameter of membrane (m)
d_o	outside diameter of membrane (m)
D	diffusion coefficient of carbon dioxide in the liquid-phase ($m^2\,s^{-1}$)
D_i	isopropyl alcohol density (kg/m^3)
D_p	polymer density (kg/m^3)
D^*	geometric mean diameter (nm)
$f(d)$	pore size distribution function
$f_f(d)$	pore flux distribution function
H	Henry's constant
k_g	individual mass-transfer coefficient of gas phase ($m\,s^{-1}$)
k_l	individual mass-transfer coefficient of liquid-phase ($m\,s^{-1}$)
k_m	individual mass-transfer coefficient of membrane ($m\,s^{-1}$)
K_{ol}	overall mass-transfer coefficient ($m\,s^{-1}$)
l_m	thickness of the hollow fiber (m)
L	effective length of the membrane module (m)
Q_l	liquid volumetric flow rate ($m^3\,s^{-1}$)
R	correlation coefficient
$R(a)$	rejection coefficient of a solute with diameter a for a membrane
Re	Reynold number
Sc	Schmidt number
Sh	Sherwood number

V	velocity ($m\,s^{-1}$)
w_1	weight of the wet membrane (kg)
w_2	weight of the dry membrane (kg)

Greek letters

α	constant
β	constant
ε_m	porosity of the membrane
σ	geometric standard deviation
τ_m	tortuosity of the membrane

References

[1] A. Gabelman, S. Hwang, Hollow fiber membrane contactors, J. Membr. Sci. 159 (1999) 61–106.

[2] J.L. Li, B.H. Chen, Review of CO_2 absorption using chemical solvent in hollow fiber membrane contactors, Sep. Purif. Technol. 41 (2005) 109–122.

[3] B. Li, K.K. Sirkar, Novel membrane and device for vacuum membrane distillation-based desalination process, J. Membr. Sci. 257 (2005) 60–75.

[4] C. Feng, R. Wang, B. Shi, G. Li, Y. Wu, Factors affecting pore structure and performance of poly(vinylidene fluoride-*co*-hexafluoro propylene) asymmetric porous membrane, J. Membr. Sci. 277 (2006) 55–64.

[5] S. Karoor, K.K. Sirkar, Gas absorption studies in microporous hollow fiber membrane modules, Ind. Eng. Chem. Res. 32 (1993) 674–684.

[6] M. Khayet, C.Y. Feng, K.C. Khulbe, T. Matsuura, Study on the effect of non-solvent additive on the morphology and performance of ultrafiltration hollow fiber membranes, Desalination 148 (2002) 321–327.

[7] M. Khayet, The effects of air gap length on the internal and external morphology of hollow fiber membranes, Chem. Eng. Sci. 58 (2003) 3091–3104.

[8] M.L. Yeow, Y.T. Liu, K. Li, Morphological studies of poly(vinlylidene fluoride) asymmetric membranes: effect of the solvent, additive and the dope temperature, J. Appl. Polym. Sci. 92 (2004) 1782–1789.

[9] H. Mahmud, A. Kumar, R.M. Narbaitz, T. Matsuura, A study of mass transfer in the membrane air-stripping process using microporous polypropylene hollow fibers, J. Membr. Sci. 179 (2000) 29–41.

[10] H.A. Rangwala, Absorption of carbon dioxide into aqueous solutions using hollow fiber membrane contactors, J. Membr. Sci. 112 (1996) 229–240.

[11] R. Prasad, K.K. Sirkar, Dispersion-free solvent extraction with microporous hollow-fiber modules, AIChE J. 34 (1988) 177–188.

[12] M. Mavroudi, S.P. Kaldis, G.P. Sakellaropoulos, A study of mass transfer resistance in membrane gas–liquid contacting processes, J. Membr. Sci. 272 (2006) 103–115.

[13] K.K. Sirkar, Other new membrane processes, in: W.S.W. Ho, K.K. Sirkar (Eds.), Membrane Handbook, Chapman & Hall, New York, 1992, pp. 885–899.

[14] Z. Qi, E.L. Cussler, Microporous hollow fibers for gas absorption. I. Mass transfer in the liquid, J. Membr. Sci. 23 (1985) 321–332.

[15] R. Wang, H.Y. Zhang, P.H.M. Feron, D.T. Liang, Influence of membrane wetting on CO_2 capture in microporous hollow fiber membrane contactors, Sep. Purf. Technol. 46 (2005) 33–40.

[16] M.C. Yang, E.L. Cussler, Designing hollow-fiber contactors, AIChE J. 32 (11) (1986) 1910–1916.

[17] S.R. Wickramasinghe, M.J. Semmens, E.L. Cussler, Mass transfer in various hollow fiber geometries, J. Membr. Sci. 69 (1992) 235–250.

[18] J. Ren, R. Wang, H. Zhang, Zh. Li, D. Liang, J. Tay, Preparation and characterization of asymmetric poly(vinylidene fluoride) (PVDF) hollow fiber membranes for CO2 capture, J. Membr. Sci. 281 (2006) 334–344.

[19] J.G. Wijmans, J.P.B. Baaij, C.A. Smolders, The mechanism of formation of microporous of skinned membrane produced by immersion precipitation, J. Membr. Sci. 14 (1983) 263–274.

[20] H.Y. Zhang, R. Wang, D.T. Liang, Modelling and experimental study of CO_2 absorption in hollow fiber membrane contactors, J. Membr. Sci. 279 (2006) 301–310.

[21] E. Fontananova, J.C. Jansen, A. Cristiano, E. Curcio, E. Drioli, Effect of additives in the casting solution on the formation of PVDF membranes, Desalination 192 (2006) 190–197.

[22] L.R. Fisher, R.A. Gamble, J. Middlehurst, The Kelvin equation and the capillary condensation of water, Nature 290 (1981) 575–576.

[23] M. Khayet, C.Y. Feng, K.C. Khulbe, T. Matsuura, Preparation and characterization of polyvinylidene fluoride hollow fiber membranes for ultrafiltration, Polymer 43 (2002) 3879–3890.